OPEN

Correspondence and
requests for materials
should be addressed to
K.F.Y. (kfyao@
tsinghua.edu.cn)

Highly Uniform and Reproducible Surface Enhanced Raman Scattering on Air-stable Metallic Glassy Nanowire Array

Xue Liu, Yang Shao, Yao Tang & Ke-Fu Yao

School of Materials Science and Engineering, Tsinghua University, Beijing, People's Republic of China.

Preparation of surface enhanced Raman scattering (SERS) nanostructures with both high sensitivity as well as high reproducibility has always been difficult and costly for routine SERS detection. Here we demonstrate air-stable metallic glassy nanowire arrays (MGNWAs), which were prepared by a cheap and rapid die nanoimprinting technique, could exhibit high SERS enhancement factor (*EF*) as well as excellent reproducibility. It shows that $Pd_{40.5}Ni_{40.5}P_{19}$ MGNWA with nanowires of 55 nm in diameter and 100 nm in pitch possesses high SERS activity with an *EF* of 1.1×10^5, which is 1–3 orders of magnitudes higher than that of the reported crystal Ni-based nanostructures, and an excellent reproducibility with a relative standard deviation of 9.60% measured by 121 points over an area of 100 μm*100 μm. This method offers an easy, rapid, and low-cost way to prepare highly sensitive and reproducible SERS substrates and makes the SERS more practicable.

D etection of trace amounts of molecules is a longstanding challenge in catalysis, biology, biomedicine and molecular nanotechnology. Surface enhanced Raman scattering (SERS) provides a powerful non-destructive spectroscopy technique for such identification, which is comparable to single-molecule fluorescence spectroscopy but without suffering from rapid photobleaching[1–3]. By employing surface plasmon polariton resonance occurring in the vicinity of the metal surface, especially narrow nanogaps between sharp corners and edges of metallic nanostructures, namely "hot spots"[3–5], the sensitivity of SERS can reach single molecular level[3]. Applicable SERS substrates require both high enhancement factor (*EF*) and excellent spatial reproducibility[5,6]. However, although very high *EF* can be achieved and several SERS substrates with signal relative standard deviation (RSD) less than 7% were reported[7–9], commonly used substrates based on metals, either prepared by corrosion or sol-gel methods, show very poor reproducibility with fluctuant *EFs* that may vary across several orders of magnitudes, which severely hinders the applications of SERS[6,10,11]. A number of efforts have been made to improve the reproducibility of metallic substrates, most notably metallic array nanostructures where the well-ordered distribution of hot spots endows them high reproducibility[5,10–16]. But the most used metallic array nanostructures preparation techniques, such as electron beam lithography, nanosphere lithography, focused ion beam pattering, vacuum evaporation and soft-lithography, are limited by the high costs, the enormous difficulties to extend to large scales or complicated preparation steps[7,11,12,17]. Preparation of SERS metallic array nanostructures with both high sensitivity and high reproducibility still remains difficult and costly for routine SERS detection. In addition, the easy oxidation and sulfuration make the prepared SERS substrates hard to be stored[3].

Thermoplastic forming based die nanoimprinting of metallic glasses (MGs) could be a potential cheap way for mass production of metallic array nanostructures due to the net-shape forming abilities of MGs. Very recently, it was reported that with inexpensive templates such as anodic aluminum oxide (AAO), metallic glassy nanowire arrays (MGNWAs) can be prepared by nanoimprinting technique[18–21], which is a rapid, controllable, green and one-step forming technology. What's more, MGNWAs possess better mechanical properties as well as corrosion resistance than their crystal counterparts[20,22], making them easy to be conserved and durable in application. Then it is possible to employ the MGNWAs for SERS detection. $Pd_{40.5}Ni_{40.5}P_{19}$[21,23] is a classic MG composition and possesses wide supercooled liquid region (SCLR) as well as excellent anti-oxidation properties, which endows it excellent thermoplastic forming ability. What's more, Pd and Ni possess stable SERS activity when excited by
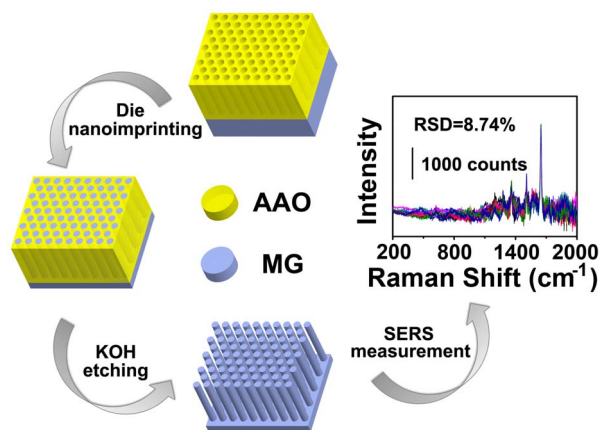
Figure 1 | Illustration of nanoimprimting process to fabricate MGNWA.

different wavelengths of light[24]. In present work, we report the preparation and demonstration of air-stable MGNWAs capable of serving as SERS substrates with high *EF* as well as excellent reproducibility by using a classic MG of $Pd_{40.5}Ni_{40.5}P_{19}$ as an example.

Results

Fabrication of MGNWAs. In order to determine the die nanoimprinting parameters, the glassy structure of the as-prepared sample was verified by X-ray diffraction (XRD), and then the T_g and T_x were indexed as 574 K and 666 K by differential scanning calorimetry (DSC), respectively. The XRD spectrum and DSC curve can be found in Supplementary Fig. S1. Therefore, the SCLR ΔT ($\Delta T = T_x - T_g$) of the as prepared $Pd_{40.5}Ni_{40.5}P_{19}$ glassy sample is 92 K. Thus, a typical temperature of 633 K was chosen as the processing

temperature, and a pressure of 354 MPa was applied to overcome the capillary pressure.

The illustration of the die nanoimprinting process is displayed in Fig. 1. Before the die nanoimprinting processing, the as quenched $Pd_{40.5}Ni_{40.5}P_{19}$ MG sample was cut into specimens with thickness of 3 mm using MTI 150 low speed diamond saw. Then the specimens were polished at the end surfaces to create fresh surfaces for nanoimprinting. After that the MG specimen was assembled abutting against an AAO template in a $\Phi6$ mm steel die mould. The AAO template was purchased from Shanghai Shangmu Technology Co. Ltd. with hole diameter of ~55 nm, depth of ~1 μm and pitch of ~100 nm (seeing Supplementary Fig. S2). The steel die mould with the MG specimen and the AAO template was subsequently placed on a heating plate that has been heated to 633 K, and held for 1 min to homogenize the temperature. Then the MG specimen was die nanoimprinted into the AAO template with a certain pressure and held for several minutes to make the MG fill into the nanopores of the AAO template. Finally, the MGNWA with a diameter of 6 mm was released by dissolved the AAO template in KOH solution after die nanoimprinting and then the SERS activity was measured.

Characterizations of MGNWAs. After die nanoimprinted under 354 MPa at 633 K for 3 min, MGNWA with segregated nanowires (NWs) (hereinafter to be referred as "s-type MGNWA") was prepared. The XRD spectrum of the sample is shown in Fig. 2a, in which no sharp diffraction peak can be found, revealing that there is no obvious crystallization occurred during the die nanoimprinting process. Fig. 2b exhibits the scanning electron microscope (SEM) image of the s-type MGNWA, where most NWs are segregated from each other. It can be seen that the NWs were distributed fairly uniformly on the whole die nanoimprinted surface and possess short range order in micrometer scale. Some "white dots" are noticed in Fig. 2b, which are proved to be clusters of aggregated
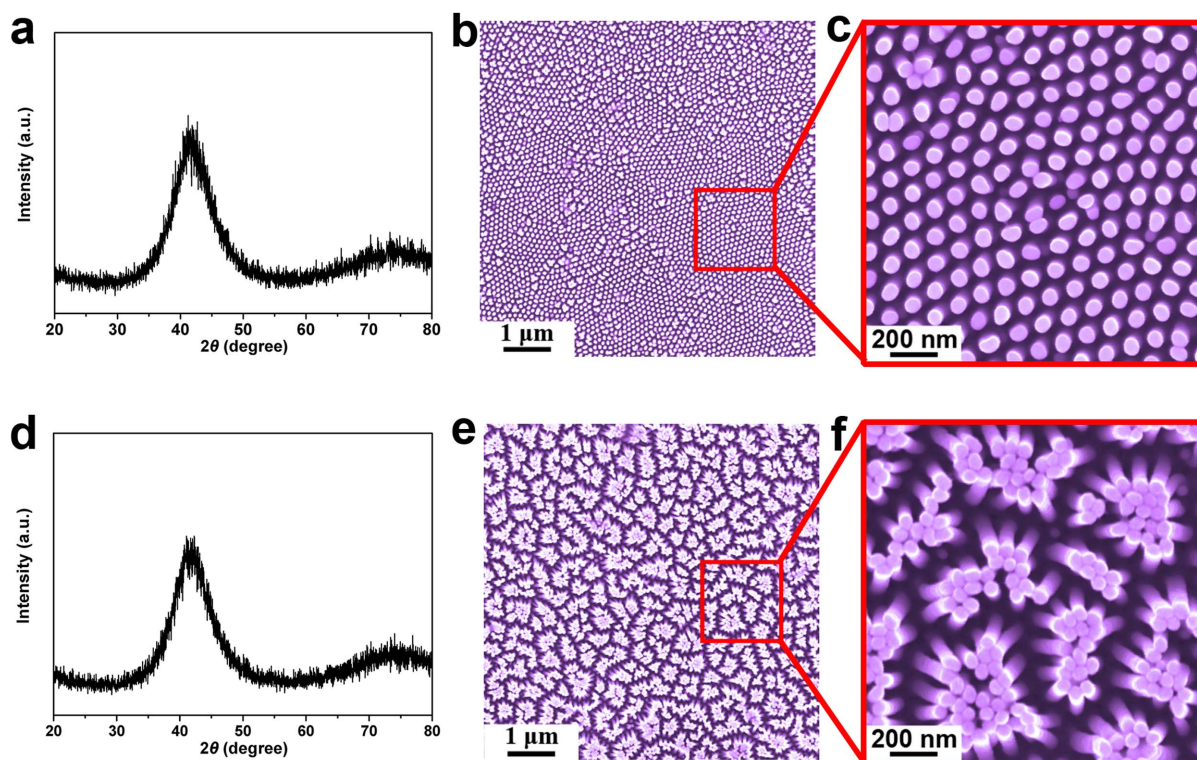

Figure 2 | XRD spectra and SEM images of the die nanoimprinted $Pd_{40.5}Ni_{40.5}P_{19}$ MGNWAs. (a) XRD spectrum of the sample die nanoimprinted under 354 MPa at 633 K for 3 min. (b) SEM image of the s-type MGNWA. (c) High-magnification image of the area marked by red square in (b). (d) XRD spectrum of the sample die nanoimprinted under 354 MPa at 633 K for 5 min. (e) SEM image of the a-type MGNWA. (f) High-magnification image of the area marked by red square in (e).
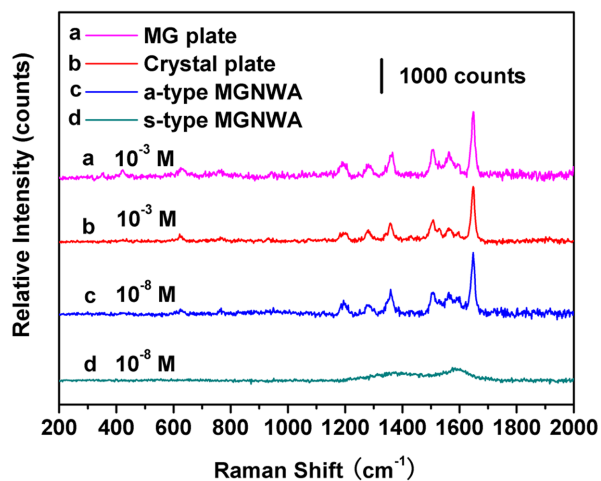
Figure 3 | SERS spectra of RhB on plates and MGNWAs. Curves a and b are Raman spectra of 10^{-3} M RhB on a $Pd_{40.5}Ni_{40.5}P_{19}$ MG plate and its crystal counterpart. Curves c and line d are SERS spectra of 10^{-8} M RhB on the a-type MGNWA and the s-type MGNWA.

2–4 NWs. A typical cluster of aggregated 4 NWs can be clearly seen in the upper left quadrant of Fig. 2c, which is the high-magnification image of the area marked with the red square in Fig. 2b. Due to the high repetition accuracy of MG, the die nanoimprinted sample inherits the features of the AAO template, such as the sections are not all perfectly circular but mainly quasi-circular. It can be found from Fig. 2c that the NWs are highly ordered within 1–2 μm, and the feature NW diameter as well as the pitch of the s-type MGNWA are measured to be 55 nm and 100 nm, respectively, which is consistent with the AAO template.

By extending the die nanoimprinting time to 5 min, MGNWA with aggregated NWs (hereinafter to be referred as "a-type MGNWA") was prepared, and the XRD spectrum is shown in Fig. 2d. No sharp diffraction peak could be observed in the spectrum, indicating that the a-type MGNWA is still amorphous. The SEM image in Fig. 2e reveals that tens of NWs are aggregated together to form NW bundles in the a-type MGNWA, and those NW bundles are also distributed fairly uniformly on the whole die nanoimprinted surface beyond micron scale, as shown in Supplementary Fig. S3. The high-magnification image of the area marked with the red square in Fig. 2e is shown in Fig. 2f, in which the NWs in one bundle are aggregated on the tips. It is due to that the lengths of the NWs increase with the extension of die nanoimprinting time, which leads to the increasing of the aspect ratio. And the increasing of aspect ratio makes the NWs easily destabilized, resulting in that the NWs prefer to aggregate together to reduce the entire surface thereby decreasing the surface energy.

SERS activities of MGNWAs. After keeping in ambient air for ten months, the morphologies of MGNWAs samples didn't change and no obvious oxidation was observed through SEM inspection, indicating that the MGNWAs samples possess excellent air-stability compared with the most used SERS substrate of silver particles. Then SERS activities of the MGNWAs samples were investigated.

Since the SERS on MGs substrates have never been studied before, it is necessary to figure out whether MGs perform differently in SERS activity compared with crystal metals. Due to the fact that it is quite difficult to synthesize two metallic samples with exactly identical nanostructure but one in amorphous phase and the other one in crystal phase, a $Pd_{40.5}Ni_{40.5}P_{19}$ MG plate and a counterpart crystallized plate with surfaces polished were used to compare the bulk Raman signal intensities of MG with that of its crystal counterpart. Curves a and b in Fig. 3 show the bulk Raman spectra of 10^{-3} M Rhodamine B

Table 1 | Experimental and literature SERS shifts of RhB molecules detected by MGNWA with aggregated NWs and Ag particle substrates, respectivly

Raman Shift

Experimental	Literature[25]	Assignments[25]
1648	1648	aromatic C-C stretching
1597	1595	C = C stretching
1564	1565	aromatic C-C stretching
1528	1529	--
1507	1506	aromatic C-C stretching
1432	1433	--
1358	1356	aromatic C-C stretching
1280	1280	C-C bridge-bands stretching
1198	1201	aromatic C-H bending
933	--	--
765	--	--
622	620	aromatic bending
423	--	--

(RhB) on a $Pd_{40.5}Ni_{40.5}P_{19}$ MG plate and its crystal counterpart, in which the MG plate and the crystal plate show similar Raman spectra. Taking the peak around 1648 cm^{-1} into account, by applying the Lorentz fitting, the intensities of the MG plate and the crystallized plate were measured to be 1990 counts and 1737 counts, respectively. Although the surfaces were polished, there also exist some hot spots, therefore the bulk Raman spectra shown in curves a and b are also SERS spectra. This result indicates that the SERS activity of MG substrate is better than that of their crystalline counterparts.

To evaluate the SERS properties of the two types of MGNWAs prepared above, RhB aqueous solution with concentration of 10^{-8} M was used, and the SERS spectra are shown in curves c and d in Fig. 3. There are only two broadening peaks can be seen by using the s-type MGNWA as substrate, while a typical SERS spectrum with plenty of peaks can be seen by using the a-type MGNWA as substrate. The SERS spectrum of RhB molecules on the a-type MGNWA completely resembles the spectral features of that on Ag particles[25] with inappreciable frequency shifts, as shown in Table 1. It can be found that most Raman shifts and the corresponding assignments agree well with the literature report and only several weak Raman shifts have no accurate assignments, such as the Raman shifts of 933, 765, and 433 cm^{-1}.

It is obvious that the a-type MGNWA possesses better SERS activity. To quantify the SERS activity of the a-type MGNWA, *EF* was calculated by comparing the intensity of a single molecule from the SERS signal with that from the bulk Raman signal by the formula[4]

$$EF = (I_{SERS}/N_{SERS})/(I_R/N_R) \qquad (1)$$

where I_{SERS} and I_R are the intensities of the selected scattering bands in the SERS and bulk Raman spectra, respectively, N_{SERS} is the number of probe molecules contributing to the SERS signal, and N_R is the number of probe molecules contributing to the bulk Raman signal. Assuming that the probed molecules are distributed on the substrates uniformly[4], the number of probe molecules contributing to the signal N can be estimated by

$$N = N_A \times C \times V_{droplet}/A_{spot} \times A_{laser} \qquad (2)$$

where N_A is the Avogadro's number, C is the concentration of the used RhB, $V_{droplet}$ is the volume of the RhB droplet, A_{spot} is the area of the spot formed by the RhB droplet, and A_{laser} is the area of the laser spot. Since the specimens for SERS and bulk Raman tests are prepared in the same way and measured with the same parameters (seeing the methods), equation (1) can be written as

$$EF = (I_{SERS}/I_R)/(N_R/N_{SERS}) \qquad (3)$$

Table 2 | Parameters for the calculation of *EF*

Spectra	C (mol·L^{-1})	Relative intensity (counts)		EF	
		1648 (cm^{-1})	1358 (cm^{-1})	1648 (cm^{-1})	1358 (cm^{-1})
SERS	10^{-8}	627	1792	1.2 × 10^5	1.0 × 10^5
Bulk Raman	10^{-3}	509	1737		

$$= (I_{SERS}/I_R)/(C_R/C_{SERS}) \qquad (4)$$

where C_R and C_{SERS} are the concentrations of the RhB on crystal plate and the a-type MGNWA, respectively. Taking the two strongest peaks of 1648 cm^{-1} and 1358 cm^{-1} into account, the relevant data required by equation (4) are listed in Table 2. The *EF* is calculated to be about 1.2 × 10^5 and 1.0 × 10^5 by using the peaks of 1648 cm^{-1} and 1358 cm^{-1}, respectively, and the average *EF* is 1.1 × 10^5, which is 1–3 orders of magnitudes higher than that of the reported crystal Ni- or Pd-based NWs[15,26,27] and comparable to that of gold metamaterials and nanostar arrays[5,28]. It indicates that the nanostructures of MGNWA can exhibit strong SERS *EF*.

To further study the SERS property of the a-type MGNWA, a series of SERS spectra by using RhB with concentrations from 10^{-5} M to 10^{-9} M on the a-type MGNWA were measured, as displayed in Fig. 4a. The signals are found to be monotonically decreasing with the decreased concentration while the spectral features are quite alike with nearly no frequency shift. Even at a concentration as low as 10^{-9} M, the spectral features of RhB can be still seen clearly. The high sensitivity is comparable of gold and silver nanoparticles[29]. By applying the Lorentz fitting, the intensities of the peaks around 1648 cm^{-1} are measured, and the relevant data are listed in Supplementary Table S1. It is found that the SERS intensities (I_{SERS}) and the concentration of RhB (C_{RhB}) have a correlation from 10^{-5} M to 10^{-9} M as follow:

$$\lg I_{SERS} = 5.66 + 0.31 \times \lg C_{RhB} \qquad (5)$$

with an *R square* higher than 0.995, as shown in Fig. 4b. It indicates that the prepared a-type MGNWA of Pd$_{40.5}$Ni$_{40.5}$P$_{19}$ MG is very suitable to be used as quantitative sensor for μM-nM detection of small molecules such as RhB.

It has been reported that there are mainly two structures contributing to the enhancement of the Raman signal when employing NW array as substrates: one is the imperfections and irregularities presented on the NW surface[13], and the other is the NWs tips touching each other in the NW bundles[14–16]. To find out the origin of the high *EF* in the a-type MGNWA of the Pd$_{40.5}$Ni$_{40.5}$P$_{19}$ MG, the a-type MGNWA was immersed into industrial alcohol for 24 h. Then the a-type MGNWA was dried under 323 K for 30 min, and a thin organic membrane was coated on the NWs tips without significant change in the morphology of the MGNWA (seeing Supplementary Fig. S4). Then the SERS property of the coated a-type MGNWA was measured according to the steps described in the methods section and the corresponding SERS spectra are shown in Fig. 5a. It can be found that the intensity of the SERS signal on the a-type MGNWA decreases significantly after coating. Since the coating treatment only changed the conditions of the NW tips, the decreasing of SERS signal indicates that the aggregated NW tips play an important role in the enhancement effect. To further ensure the origin of the enhancement of the Raman signal, Raman mapping of a 20 μm × 20 μm with laser spot of ~0.75 μm was conducted with 10^{-6} M RhB on the coated a-type MGNWA, and the results were shown in Supplementary Fig. S5. The distribution of the high SERS signal intensity places (hot spots) corresponds very well with that of the aggregated NW tips, indicating that the enhancement of the Raman signal is mainly contributed by the aggregated NW tips.

Just like in crystal MGNWAs, there also exist localized electromagnetic fields caused by the lightning rod effect around the NW tips in MGNWAs[15,16,26]. In the a-type MGNWA, several NWs' tips attach each other, resulting the distances among them decreased significantly. Between the NW tips, there are plentiful of sub-10-nm gaps, where powerful localized electromagnetic fields exist and therefore hot spots caused by the electromagnetic enhancement are formed[30]. Due to the existence of plentiful hot spots between the NW tips, the a-type MGNWA exhibits much better SERS activity than that of the s-type MGNWA. After coating although the morphology of the a-type MGNWA doesn't change, the organic membrane separates RhB molecules from hot spots between the NW tips. Since the enhancement of the Raman signal is positively related to the electromagnetic field intensity, which falls off exponentially with the distance from the hot spot, the SERS activity of the coated a-type MGNWA
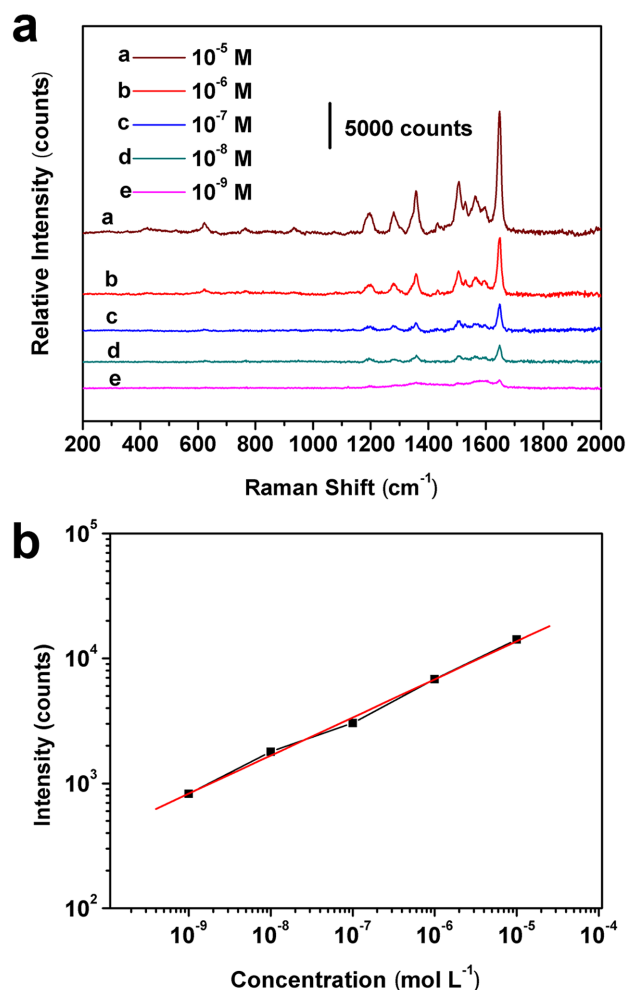

Figure 4 | SERS spectra of RhB with different concentrations on the a-type MGNWA. (a) SERS spectra of 10^{-5} M–10^{-9} M RhB (line a–e) on the a-type MGNWA. (b) The RhB concentrations *v.s.* the SERS signal intensities of the peaks around 1648 cm^{-1} measured from (a). The red line is the fitted line and the black polyline with dots is the measured data.
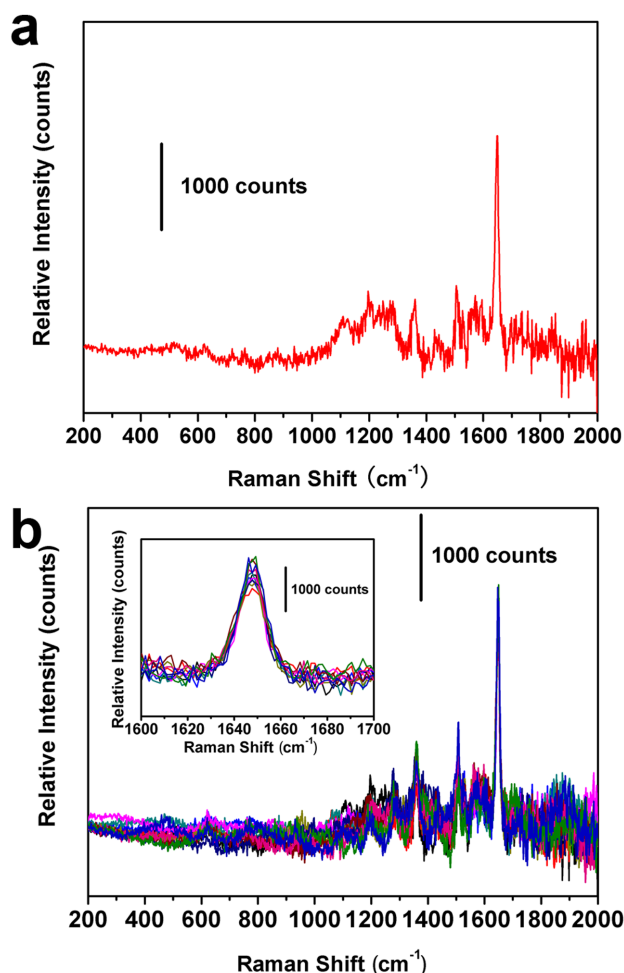
Figure 5 | (a) SERS spectra of 10^{-6} M RhB on the coated a-type MGNWAs. (b) SERS spectra of 10^{-6} M RhB from 11 randomly selected positions on the coated a-type MGNWA. Inset in (b) is the enlarged detail of the peaks around 1648 cm^{-1}.

decreases significantly due to the separation effect of the organic membrane. Hence the enhancement mechanism in MGNWAs is also mainly due to the lightning rod effect and the plentiful hot spots between the NW tips.

It is well known that the poor spatial reproducibility of Raman signals has been the main obstacle to the extensive application of SERS effect. The reproducibility is mainly related to the uniformity of the hot spots distribution. From Fig. 2b and e, it can be seen that in

micrometer scale the prepared MGNWAs are fairly uniformly therefore hot spots are also uniformly distributed. Since the diameter of the laser spot is usually in micrometer scale in SERS tests (in our test the laser spot is about 5 μm in diameter), the Raman signals from different places of the MGNWA substrates would be quite uniform. Thus it could be predicted from the microstructure that the a-type MGNWA should possess excellent SERS signal reproducibility.

It can be seen from Supplementary Fig. S4 that the morphology of the a-type doesn't change after coating, therefore the distribution of hot spots is retained. Hence the organic membrane mainly impairs the SERS activity of the a-type MGNWA, but has little influence on the uniformity of the hot spots distribution and thereby the reproducibility of the a-type MGNWA. In addition, when there is a signal intensity fluctuations, the relative changing would be stronger in the SERS spectrum with lower signal intensity. So for testing the reproducibility of the a-type MGNWA, the coated a-type MGNWA was used. Fig. 5b shows the SERS spectra of 10^{-6} M RhB collected from 11 randomly selected positions on the coated a-type MGNWA under identical experimental conditions. The relative standard deviation (RSD) of SERS peak around 1648 cm^{-1} is used to estimate the reproducibility of the SERS signals. After fitted by the Lorenz curve, the intensities of the peaks around 1648 cm^{-1} are shown in Supplementary Fig. S6, and the RSD value is calculated to be 8.74%, indicating the coated a-type MGNWA therefore the a-type MGNWA possesses excellent SERS signal reproducibility.

As further proof of the excellent reproducibility, Raman mapping of a 100 μm × 100 μm with laser spot of ~2.5 μm was conducted with 10^{-6} M RhB on the coated a-type MGNWA, and the results were shown in Fig. 6. The SERS signal intensity distributions of the bands around 1648 cm^{-1} and 1358 cm^{-1} were shown in Fig 6a and b, respectively, where the SERS signal intensity is quite uniform except few points. The Raman spectra shown in Fig. 6c also exihibit very high uniformity. The RSD was calculated to be 9.60% according to the signal intensities of the measured 121 points using the band around 1648 cm^{-1}. The relatively low RSD value declares the excellent SERS signal reproducibility of the a-type MGNWA.

Discussion

Improvement in SERS EF. We have proposed a new easy, rapid, environmental and economical method to prepare air-stable SERS substrates with high *EF* and high reproducibility by die nanoimprinting $Pd_{40.5}Ni_{40.5}P_{19}$ MG into the a-type MGNWA. The excellent reproducibility origins from the special structure of the a-type MGNWA, where the NWs are uniformly distributed. Thus as long as the uniformity of the MGNWA remains unchanged, the reproducibility of the SERS signal can be maintained. It is known that the high *EF* is affected by both the structure and the constituent elements, therefore the *EF* of the a-type MGNWA can be promoted
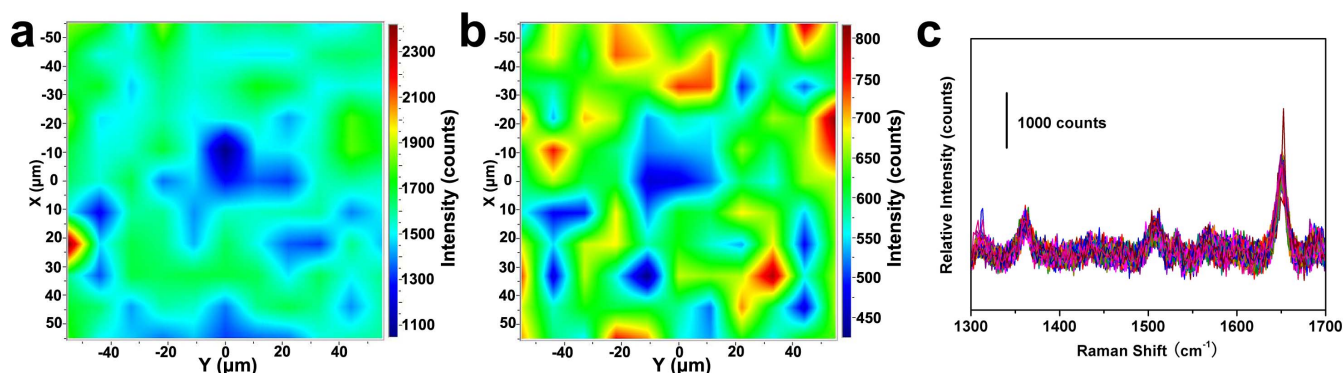

Figure 6 | Raman mapping images of (a) the bands around 1648 cm^{-1}, (b) around 1358 cm^{-1} and (c) the corresponding Raman spectra with 10^{-6} M RhB. (Laser beam power of ~25 mW, laser beam diameter of ~2.5 μm, excitation wavelength of 514 nm, scan time of 20 s, field lens of 10 times, accumulation of 1 times, mapping area of 100 μm * 100 μm and detection step of 10 μm).

by optimizing the structure and the alloy composition. In general the more hot spots there exist on unit area, the higher *EF* will be obtained. In the MGNWA structures prepared above, most hot spots are generated by the aggregated NW tips, and other parts of the NWs contribute litter to the SERS active. By applying dealloying method, the NWs can be transformed into nanoporous NWs[31], and there would be lots of new hot spots created in the surface of the NWs, therefore the *EF* would be promoted. Furthermore, it is widely known that Pd and Ni are not strong SERS active elements, and their enhancement abilities are several orders of magnitude lower than that of strong SERS active elements such as Ag, Au and Cu[16,32,33]. Thus by replacing the $Pd_{40.5}Ni_{40.5}P_{19}$ MG into other MG with strong SERS active elements, the *EF* of the SERS can be further increased with reproducibility maintained. Therefore it would open a window to prepare SERS substrates with high sensitivity and high reproducibility in a rapid and economical way by die nanoimprinting MG into MGNWAs form.

Applications in ultraviolet (UV) excited SERS. When the wavelength of the exciting light is close to the electronic absorption bands of the probe molecule, resonance Raman scattering will form and the scattering efficiency can be dramaticly enhanced due to the resonance effect[34,35]. Since the electronic absorption bands of many molecules, especially biomolecules such as DNA, are in the range of UV[35,36], the UV excited SERS have attracted more and more attentions in the recently years. What's more, the fluorescence interference can be avoided in the deep UV Raman spectroscopy[34], making the UV excited SERS more attractive. It has been reported that Pd and Ni possess much better SERS activity than that of Au, Ag and Cu under the ultraviolet excitation[24]. Thus, the prepared $Pd_{40.5}Ni_{40.5}P_{19}$ MGNWA could be applied as excellent SERS substrates in ultraviolet (UV) excited SERS for detection of trace amount of small biological molecules such as DNA.

Applications in mass production of SERS substrates. Recently it was reported that MGs are able to serve as outstanding mold inserts for hot embossing of polymers with different patterns on the surface[37], and after coated with metal the patterned shaped polymers are able to possess SERS active surface[38]. By changing the template MG nanohole arrays can be prepared by die nanoimprinting processing, therefore metallized polymer NW arrays can be easily prepared for SERS applications. It would greatly decrease the cost as well as increase the production efficiency of producing SERS substrates, and may bring SERS into widespread applications.

Conclusion

Highly uniform and air-stable MGNWAs have been fabricated by using die nanoimprinting method. The prepared $Pd_{40.5}Ni_{40.5}P_{19}$ MGNWA with nanowires of 55 nm in diameter and 100 nm in pitch possesses high SERS activity with an average *EF* of 1.1×10^5, which is 1–3 orders of magnitudes higher than that of the reported crystal Ni-based nanostructures, and an excellent reproducibility with a relative standard deviation of 9.60% measured by 121 points over an area of 100 μm*100 μm, which is much lower than those of the commonly used SERS substrates. The high SERS activity is contributed by the plentiful hot spots between the NW tips, and the excellent reproducibility originates from the uniformity of the MGNWA. The present result provides important insights into the employment of MG materials for highly sensitive and reproducible SERS applications.

Methods

Preparation of $Pd_{40.5}Ni_{40.5}P_{19}$ MG. The ingot of the studied $Pd_{40.5}Ni_{40.5}P_{19}$ alloy was prepared by melting the mixtures of high purity Pd (99.5%) and Ni (99.9%) plates and Ni_2P (99.95%) powders within a high-purity argon gas condition. The $Pd_{40.5}Ni_{40.5}P_{19}$ ingot was subsequently purified with the fluxing medium B_2O_3 in a quartz tube at about 1423 K. After purification water quenching was employed to obtain the $Pd_{40.5}Ni_{40.5}P_{19}$ bulk metallic glass sample with a diameter of 6 mm and length of 50 mm.

Characterization of MGNWA. After die nanoimprinting, the surfaces and the structures of the MGNWAs were examined by LEO1530 SEM integrated with a field emission gun and Rigaku D/max-RB XRD, respectively.

SERS measurement. RhB with analytically purity purchased from Sinopharm Chemical Reagent Co., Ltd was used as the probe molecule to study the SERS activities of the NWs. Before the SERS measurement, a 2 μL droplet of the RhB aqueous solution was dropped on each of the MGNWAs substrates which were subsequently dried at 323 K for 30 min. The solution diffused on the surface to be a spot with 0.4 cm in diameter. The SERS measurements were carried out in the center of the droplet at room temperature by a microscopic confocal Raman spectrometer (RM2000, Renishaw PLC, England) using a charge-coupled device (CCD) detector with a resolution of 1 cm^{-1}. The laser beam power was 4.7 mW and the laser beam diameter was 5 μm. Excitation wavelength of 514 nm (according to the previous literature[21]), scan time of 30 s, field lens of 20 times and accumulation of 4 times were applied. The SERS mapping measurements were carried out in the center of the droplet by a microscopic confocal Raman spectrometer (LabRAM HR Evolution, HORIBA Jobin Yvon, France) using a charge-coupled device (CCD) detector with a resolution of 0.65 cm^{-1}.

1. Zhang, R. *et al.* Chemical mapping of a single molecule by plasmon-enhanced Raman scattering. *Nature* **498**, 82–86 (2013).
2. Kinkhabwala, A. *et al.* Large single-molecule fluorescence enhancements produced by a bowtie nanoantenna. *Nat. Photonics* **3**, 654–657 (2009).
3. Liu, H. *et al.* Single molecule detection from a large-scale SERS-active Au79Ag21 substrate. *Sci. Rep.* **1**, 112; DOI:10.1038/srep00112 (2011).
4. Zhang, L., Lang, X., Hirata, A. & Chen, M. Wrinkled Nanoporous Gold Films with Ultrahigh Surface-Enhanced Raman Scattering Enhancement. *ACS Nano* **5**, 4407–4413 (2011).
5. Osinkina, L., Lohmuller, T., Jackel, F. & Feldmann, J. Synthesis of Gold Nanostar Arrays as Reliable, Large-Scale, Homogeneous Substrates for Surface-Enhanced Raman Scattering Imaging and Spectroscopy. *J. Phys. Chem. C* **117**, 22198–22202 (2013).
6. Sanchez-Gaytan, B. L. *et al.* Spiky Gold Nanoshells: Synthesis and Enhanced Scattering Properties. *J. Phys. Chem. C* **116**, 10318–10324 (2012).
7. He, D., Hu, B., Yao, Q. F., Wang, K. & Yu, S. H. Large-Scale Synthesis of Flexible Free-Standing SERS Substrates with High Sensitivity: Electrospun PVA Nanofibers Embedded with Controlled Alignment of Silver Nanoparticles. *ACS Nano* **3**, 3993–4002 (2009).
8. Yazgan, N. N., Boyaci, I. H., Temur, E., Tamer, U. & Topcu, A. A high sensitive assay platform based on surface-enhanced Raman scattering for quantification of protease activity. *Talanta* **82**, 631–639 (2010).
9. Dinish, U. S., Yaw, F. C., Agarwal, A. & Olivo, M. Development of highly reproducible nanogap SERS substrates: Comparative performance analysis and its application for glucose sensing. *Biosens. Bioelectron.* **26**, 1987–1992 (2011).
10. Lim, D. K. *et al.* Highly uniform and reproducible surface-enhanced Raman scattering from DNA-tailorable nanoparticles with 1-nm interior gap. *Nat. Nanotechnol.* **6**, 452–460 (2011).
11. Fan, M. K., Andrade, G. F. S. & Brolo, A. G. A review on the fabrication of substrates for surface enhanced Raman spectroscopy and their applications in analytical chemistry. *Anal. Chim. Acta* **693**, 7–25 (2011).
12. Que, R. H. *et al.* Highly Reproducible Surface-Enhanced Raman Scattering on a Capillarity-Assisted Gold Nanoparticle Assembly. *Adv. Funct. Mater.* **21**, 3337–3343 (2011).
13. Driskell, J. D. *et al.* The use of aligned silver nanorod Arrays prepared by oblique angle deposition as surface enhanced Raman scattering substrates. *J. Phys. Chem. C* **112**, 895–901 (2008).
14. Lee, S. J., Morrill, A. R. & Moskovits, M. Hot spots in silver nanowire bundles for surface-enhanced Raman spectroscopy. *J. Am. Chem. Soc.* **128**, 2200–2201 (2006).
15. Sauer, G. *et al.* Surface-enhanced Raman spectroscopy employing monodisperse nickel nanowire arrays. *Appl. Phys. Lett.* **88**, 023106 (2006).
16. Liao, Q. *et al.* Gold Nanorod Arrays with Good Reproducibility for High-Performance Surface-Enhanced Raman Scattering. *Langmuir* **25**, 4708–4714 (2009).
17. Liu, G. L. & Lee, L. P. Nanowell surface enhanced Raman scattering arrays fabricated by soft-lithography for label-free biomolecular detections in integrated microfluidics. *Appl. Phys. Lett.* **87**, 074101 (2005).
18. Kumar, G., Tang, H. X. & Schroers, J. Nanomoulding with amorphous metals. *Nature* **457**, 868–872 (2009).
19. Schroers, J. Bulk Metallic Glasses. *Phys. Today* **66**, 32–37 (2013).
20. Kumar, G., Desai, A. & Schroers, J. Bulk Metallic Glass: The Smaller the Better. *Adv. Mater.* **23**, 461–476 (2011).
21. Liu, X., Shao, Y., Li, J. F., Chen, N. & Yao, K. F. Large-area and uniform amorphous metallic nanowire arrays prepared by die nanoimprinting. *J. Alloy. Compd.* **605**, 7–11 (2014).
22. Yao, K. F. & Zhang, C. Q. Fe-based bulk metallic glass with high plasticity. *Appl. Phys. Lett.* **90**, 61901 (2007).
23. Yao, K. F. & Kui, H. W. Evidence of a two-dimensional nucleation and growth mechanism for metastable nanocrystals embedded in Pd40.5Ni40.5P19 glass. *Appl. Phys. Lett.* **77**, 2313–2315 (2000).

24. Tian, Z. Q., Yang, Z. L., Ren, B. & Wu, D. Y. SERS from transition metals and excited by ultraviolet light. *Surface-Enhanced Raman Scattering: Physics and Applications* **103**, 125–146 (2006).
25. Zhang, J. T., Li, X. L., Sun, X. M. & Li, Y. D. Surface enhanced Raman scattering effects of silver colloids with different shapes. *J. Phys. Chem. B* **109**, 12544–12548 (2005).
26. Krishnadas, K. R., Sajanlal, P. R. & Pradeep, T. Pristine and Hybrid Nickel Nanowires: Template-, Magnetic Field-, and Surfactant-Free Wet Chemical Synthesis and Raman Studies. *J. Phys. Chem. C* **115**, 4483–4490 (2011).
27. Hu, J. W. *et al.* Surface-Enhanced Raman Scattering on Uniform Pd and Pt Films: From III-Defined to Structured Surfaces. *J. Phys. Chem. C* **117**, 24843–24850 (2013).
28. Wen, X. L. *et al.* Transparent free-standing metamaterials and their applications in surface-enhanced Raman scattering. *Nanoscale* **6**, 132–139 (2014).
29. Luo, L. B. *et al.* Surface-enhanced Raman scattering from uniform gold and silver nanoparticle-coated substrates. *J. Phys. Chem. C* **113**, 9191–9196 (2009).
30. Liu, T. Y. *et al.* Functionalized arrays of Raman-enhancing nanoparticles for capture and culture-free analysis of bacteria in human blood. *Nat. Commun.* **2**, 1546 (2011).
31. Mukherjee, S. *et al.* Tunable Hierarchical Metallic-Glass Nanostructures. *Adv. Funct. Mater.* **23**, 2708–2713 (2013).
32. Tian, Z. Q., Ren, B. & Wu, D. Y. Surface-enhanced Raman scattering: from noble to transition metals and from rough surfaces to ordered nanostructures. *J. Phys. Chem. B* **106**, 9463–9483 (2002).
33. Li, J. F. *et al.* Shell-isolated nanoparticle-enhanced Raman spectroscopy. *Nature* **464**, 392–395 (2010).
34. Sun, M. T. *et al.* Near- and Deep-Ultraviolet Resonance Raman Spectroscopy of Pyrazine-Al-4 Complex and Al-3-Pyrazine-Al-3 Junction. *J. Phys. Chem. C* **113**, 19328–19334 (2009).
35. Sigle, D. O., Perkins, E., Baumberg, J. J. & Mahajan, S. Reproducible Deep-UV SERRS on Aluminum Nanovoids. *J. Phys. Chem. Lett.* **4**, 1449–1452 (2013).
36. Muntean, C. M., Salehi, M., Niebling, S. & Walkenfort, B. The influence of divalent metal ions on low pH induced LacDNA structural changes as probed with UV resonance Raman spectroscopy. *J. Raman Spectrosc.* **44**, 1693–1699 (2013).
37. Ma, J., Zhang, X. & Wang, W. H. Metallic glass mold insert for hot embossing of polymers. *J. Appl. Phys.* **112** (2012).
38. Acevedo, D. *et al.* SERS Active Surface in Two Steps, Patterning and Metallization. *Adv. Eng. Mater.* **15**, 325–329 (2013).

Acknowledgments

Author contributions

K.F.Y. designed the study. X.L. fabricated samples and performed the characterizations of the samples. X.L. and Y.T. implemented the SERS experiments. All authors contributed to discussions and analysis of the data. X.L., Y.S. and K.F.Y. wrote the manuscript, with support from Y.T.

Additional information

Supplementary information accompanies this paper at http://www.nature.com/scientificreports

Competing financial interests: The authors declare no competing financial interests.

How to cite this article: Liu, X., Shao, Y., Tang, Y. & Yao, K.-F. Highly Uniform and Reproducible Surface Enhanced Raman Scattering on Air-stable Metallic Glassy Nanowire Array. *Sci. Rep.* **4**, 5835; DOI:10.1038/srep05835 (2014).